CANADIAN JOURNAL of EXPLORATION GEOPHYSICS
VOL. 38, NO. 1 (June 2013), P. 15-20

Short Note: Seismic-Q Estimation Using Full Waveform Inversion of Noisy Data – A Feasibility Study

Laurence R. Lines[1], Fereidoon Vasheghani[2], and R. Phillip Bording[3]

[1]Department of Geoscience, University of Calgary, Calgary, Alberta, Canada T2N 1N4

[2]Formerly Department of Geoscience, University of Calgary, Calgary, Alberta, Canada T2N 1N4; now ConocoPhillips, Calgary, Alberta, Canada

[3]Department of Geosciences, University of Tulsa, Tulsa, Oklahoma, USA

Abstract

The estimation of fluid viscosity in heavy oil fields is essential for optimizing enhanced oil recovery. Recent studies have examined methods for determining heavy oil fluid viscosity using seismic-Q estimation and rock physics. These Q estimation techniques have used seismic-Q tomography, as in Vasheghani and Lines (2012). While tomography can produce worthwhile results, full waveform inversion (FWI) can provide improved images by improving the tomography results. FWI is considered the most general inversion method; however, it is susceptible to difficulties associated with noisy input data. In this study, we examine the effects of additive noise on FWI for modest signal-to-noise ratios. It is shown that FWI is robust for noisy data, since the noise does not shift the position of the objective function's local minimum from the noise-free case.

Introduction

Accurate estimation of oil viscosity is essential for reliable simulation of fluid flow in heavy oil fields. Recent studies by Vasheghani and Lines (2009, 2012) have shown that viscosity estimation can be obtained by the use of crosswell seismic tomography and rock physics. A complete description of the viscosity estimation methodology has been presented in the Ph.D. thesis of Vasheghani (2011). Vasheghani's method is based on the seismic tomography techniques of Quan and Harris (1997) and the Biot squirt flow theory (BISQ), as described by Dvorkin and Nur (1993). Seismic tomography is used to provide tomograms of seismic-Q while BISQ is used to convert seismic-Q estimates to viscosity estimates. While the mapping from Q to viscosity is not unique, constraints on the range of viscosity can be used to provide the best estimate of viscosity between wells (Vasheghani and Lines, 2012).

In the estimation of Q, seismic tomography is generally done in two steps as described by Quan and Harris (1997). The first step is traveltime inversion, in which picked seismic traveltimes are matched by ray-traced traveltimes through adjustment of seismic velocities. The traveltime inversion produces the velocity tomogram and the distance matrix describing the distance of ray paths in the velocity cells, both of which are used in the second step of Q-tomography. For this second step, the Quan-Harris Q-tomography method is used.

While seismic traveltime + attenuation tomography can reliably estimate seismic-Q, it is not necessarily the final step in the inversion process. Tomography can be followed by full wave inversion to improve the accuracy of the inversion. This FWI improvement of tomography results was demonstrated for crosswell data by Zhou et al. (1993) who compared tomographic and full waveform inversion solutions to sonic logs. While tomography produced an answer "in the ballpark", full waveform inversion improved the answer. Hence, tomography and FWI inversion methods are sequential and symbiotic.

A potential problem with FWI is its ability to invert data that is contaminated with noise. Full waveform inversion treats all recorded data as signal that is related to properties of the Earth's interior. However, this FWI assumption may not always be valid, due to signal contamination from sources such as wind noise, instrument noise, traffic noise, or wave noise (in the case of marine recording). These noise sources may be unrelated to properties of the Earth's interior. In this study, we test a simple inversion algorithm for Q-estimation for data that has modest amounts of additive noise. While this testing is not the final word, a failure of these noise tests would not be a favorable FWI performance indicator.

Methodology

The inversion for seismic-Q is best done with borehole measurements such as vertical seismic profiling (VSP) data or crosswell data. For these borehole data the measurements of seismic attenuation are done in-situ on transmitted arrivals - with less ambiguity in the ray paths than with surface measurements of reflections. For borehole estimation of Q, there are two popular frequency-domain methods. One is the spectral ratio method of Spencer et al. (1982) that uses ratios of amplitude spectra for receivers at different depths. A second method of Quan and Harris (1997) examines the frequency shift in the centroid of amplitude spectra as a function of receiver position. Our experience has shown that these two methods produce similar results but that the centroid frequency method may be more robust in noisy environments.

In our tomographic inversion we intend to estimate Q, the quality factor, which is inversely proportional to the attenuation.

Q is defined as the ratio of energy of a wave over the loss of energy per cycle multiplied by 2π (Aki and Richards, 2002).

$$Q = \frac{2\pi E}{\Delta E} \tag{1}$$

In terms of the absorption coefficient, α, of waves that have a spatial decay of $e^{-\alpha x}$ (where x is distance travelled), it is shown in Toksoz and Johnston (1981) that Q can be expressed as:

$$Q = \frac{\pi}{\alpha\lambda} = \frac{\pi f}{\alpha V} \tag{2}$$

Therefore it can be seen from equation (2) that Q is dependent on absorption, velocity and frequency. The tomographic solution for Q starts with traveltime tomography in which we solve for velocity. Traveltime tomography has been described by McMechan (1983) and basically involves the solution of traveltime equations of the form:

$$t_i = \sum_j \ell_{ij} s_j \ . \tag{3}$$

Here t_i is the traveltime for the ith ray, ℓ_{ij} is the distance of the ith ray in the jth cell and s_j is the slowness (reciprocal velocity) of the jth cell. This produces a set of velocity cells, and a set of ray traced distances, ℓ_{ij} in the ray trace modeling.

Attenuation tomography is the second step in this process and for these purposes we use the algorithm proposed by Quan and Harris (1997). As the rays travel in each cell, there is attenuation of wave amplitudes and a lowering of the frequency content as the waves propagate from source to receiver. The degree of the frequency lowering can be measured and related to the attenuation. The change in the frequency content of the signal is quantified by the decrease of its centroid frequency as the wave travels from source to receiver, where the centroid frequency $\overline{f}$ for a signal's amplitude spectrum, $A(f)$ is defined as:

$$\overline{f} = \frac{\int_0^\infty fA(f)\,df}{\int_0^\infty A(f)\,df} \ . \tag{4}$$

Variation of the centroid frequency for a signal travelling from source to receiver is related to the attenuation coefficient of all cells using the following tomographic equation from Quan and Harris (1997):

$$\sum_j \ell_{ij}\alpha_{0,j} = \frac{\overline{f}_s - \overline{f}_R}{\sigma_s^2} \tag{5}$$

where subscripts i and j denote the ray cell numbers respectively, $\alpha_{0,j}$ is the attenuation coefficient in the jth cell, $\overline{f}_s$ and $\overline{f}_R$ are the centroid frequencies at the source and receiver locations, respectively, and σ_s^2 is the variance of the source signal spectrum. For computational convenience, Quan and Harris (1997) define their attenuation, $\alpha_{0,}$ to be related to the usual attenuation coefficient, α , by the linear relationship, $\alpha = \alpha_{0,} f$. We note that $\alpha_{0,}$ has the dimensions of slowness (namely T/L where L=Length, T=time).

The values of the velocities from traveltime tomography and the values of the $\alpha_{0,}$ coefficients from attenuation tomography can be combined to produce a Q tomogram by the relationship:

$$Q = \frac{\pi}{\alpha_0 V} \ . \tag{6}$$

At this point, the Q tomogram can be converted to a viscosity tomogram by using the BISQ rock physics and constraints from well information. However, given the tomography + FWI results shown by Zhou et al. (1993), we may want to go one step further and do a full waveform inversion.

In full waveform inversion, the goal is to produce a model whose response provides a good fit to all the digital amplitude values in a seismic trace. In mathematical terms, the goal is to minimize some objective function measuring differences between the observed wavefield, $u(y_{rs},t)$ and the modeled wavefield, $g(y_{rs},t)$, where y_{rs} denotes the location of the receiver, r, for a given source point, s, and t denotes the time sample. Shin (1988) and Pica et al. (1990) used the least squares objective function to do FWI. That is, the following norm, S, is minimized.

$$S = \sum_r \sum_t \left\| u\ (y_r,t) - g(y_r,t) \right\|^2 \tag{7}$$

Necessary criteria for minimization of S require that $\frac{\partial S}{\partial \theta_j} = 0$ for all of the model parameters θ_j (velocity cells, Q values, …). As shown by Lines and Treitel (1984), this minimization leads to a series of ill-posed equations of the form:

$$\mathbf{Ax = b} \tag{8}$$

Here **A** is the n by p Jacobian matrix, for n data values and p parameter values, whose elements are given by $A_{ij} = \frac{\partial g_i}{\partial \theta_j}$; **x** is the parameter change vector with values $x_j = \theta_j - \theta_j^0$, and $\mathbf{b=u-g^0}$ is the discrepancy vector between the data vector,**u**, and the vector containing the initial model response values, $\mathbf{g^0}$. This least squares form of full waveform inversion can be successful under the following conditions.

1. The form of the wave equation used to compute the modeled wavefield $g(x_{rs},t)$ is appropriate for the recorded data, $u(x_{rs},t)$.
2. We have the appropriate number of parameters, θ_j (velocity cells, Q values, block locations) to minimize S using the necessary criteria that $\frac{\partial S}{\partial \theta_j} = 0.$,
3. We have an immense amount of computer power to minimize S for a realistic number of traces and digitized times.
4. The observed seismic data are dominated by signals caused by changes in the Earth's interior and are not corrupted by noise.

With the advent of parallel processing and ever increasing computation power, conditions 1-3 are being met and worthwhile results have been shown. Condition 4 relates more to the signal-to-noise ratio in our data which may have a deleterious effect on full waveform inversion. Both coherent and incoherent noise will pose a problem for waveform inversion, as pointed out by Shin et al. (2007). In addressing the noise difficulties for the seismic-Q estimation, we perform some simple noise tests

on synthetic data. While these tests may not be definitive, if the results are not favorable, full waveform inversion would appear to be problematic in noisy environments.

Analysis and Results

For our tests, we use a model shown in Figure 1 from the paper by Vasheghani and Lines (2009). The model is a two-layer system with the real part of the impedance (density*velocity) being the same in both layers and being equal to 1,500,000 kg/m^2-s (velocity = 1500 m/s and density = 1000 kg/m^3), but with Q=210,000 (the Q for water) in the top layer and Q=6.28 (about 2π) in the second layer. The model has 120 by 120 grid points with cell sizes being 10m. The boundary between layers is located at the base of row 40. The model and the geometry of sources and receivers is also shown in Figure 1. The shot is located at grid point (60,30). The line of receivers is in every column in row 45; giving a receiver spacing is 10m. The seismic finite-difference modeling codes of Carcione (2007) have been used in these computations.

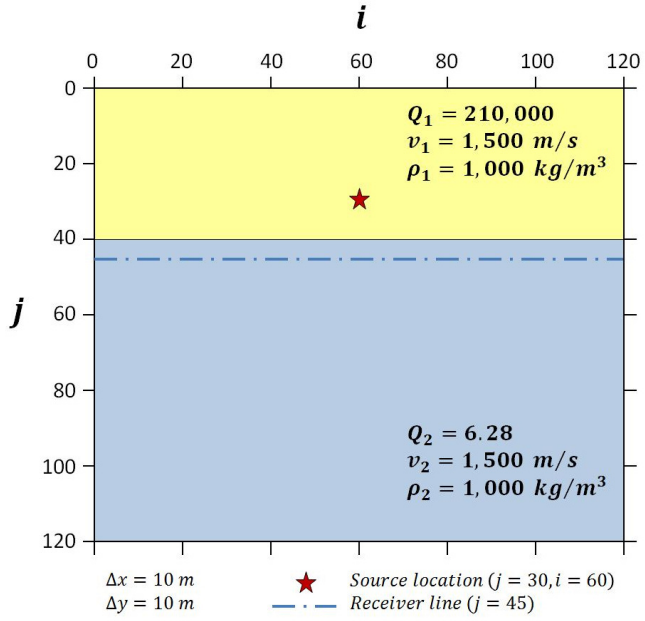

Figure 1. The model is for a synthetic seismogram of 120 by 120 grid points, with grid points separated by 10m. Layer 1 (yellow) has Q=210000 in rows 1-40 and Layer 2 (blue) has Q=6.28. The density is equal to 1000 kg/m^3 for both layers and the velocity is equal to 1500 m/s for both layers. The source position denoted as the star is at grid point (60,30) and a line of receivers is located at row 45 (just below the layer interface) with receivers at every column in the grid.

The seismogram will be dominated by transmitted first arrivals with hyperbolic shape followed closely by a reflected arrival (caused by Q-contrasts) with a short delay time. The noise-free model response is shown as the left most seismogram of Figure 2. To simulate noisy data, we add a series of random numbers to the noiseless signals. These random numbers have a standard deviation that is 0.2 as large as the standard deviation of the signal, giving us a signal-to-noise ratio of 5.0 for the noisy traces on the right hand side of Figure 2.

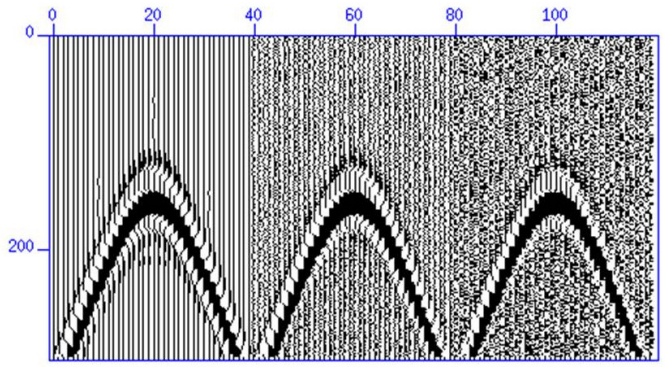

Figure 2. The seismic traces used in the FWI testing. The display shows the first 300 samples (300 ms) for every second trace for t grid points 40-119. Traces 0-39 show the noiseless seismogram for the model and shooting geometry of Figure 1; Traces 40-79 show a noisy seismogram (S/N ratio =5) and traces 80-119 show the very noisy seismogram (S/N ratio =2.5). Sample interval =1ms. Trace spacing in display = 20m.

First we consider the case of inverting a noiseless seismogram. If we choose an incorrect initial guess for Q in layer 2 as being Q^0=15 rather than Q=6.28, we obtain the seismogram for the initial guess as being the middle seismogram in Figure 3. We then invert for values of Q by iteratively solving equation (8) for the parameter change, **x**, and updating Q using $Q=Q^0+\mathbf{x}$. We continue to invert for Q by iteratively solving (8) and continuing to update Q until S in equation (7) is acceptably small. The convergence to an acceptable answer of Q=6.09 takes only 3 iterations and is outlined by Table 1. The decrease in the value of S is also shown in Table 1. The modeled seismogram for the converged answer, as shown by the right hand seismogram in Figure 3, is almost identical to the data. Hence, the inversion works well for the case of noiseless data.

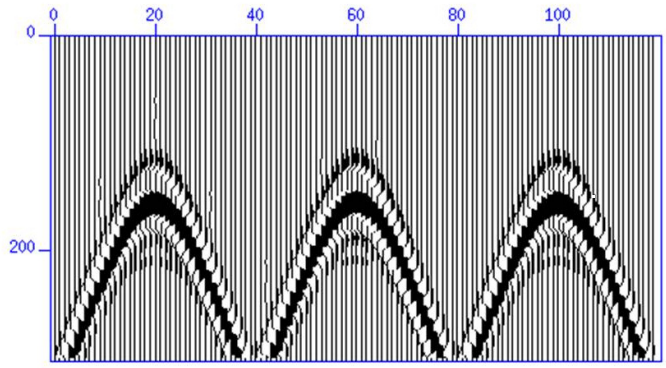

Figure 3. Traces 0-39 show the noise-free model data used in the initial test; Traces 40-79 where Q=6.28. Traces 40-79 show the model response of the initial guess of Q=15; (right) and traces 80-119 show the converged result of inversion after 3 iterations with Q=6.09. The inversion result is nearly identical to the data.

The question that then arises is one related to noise. How does additive noise affect the inversion solution? In other words, if we replace the data vector **u** by a vector of data plus noise, **u + n**, will the inversion be seriously affected? We try this for a additive noise in which the signal-to-noise ratio is S/N =5 and then for the case where S/N=2.5.

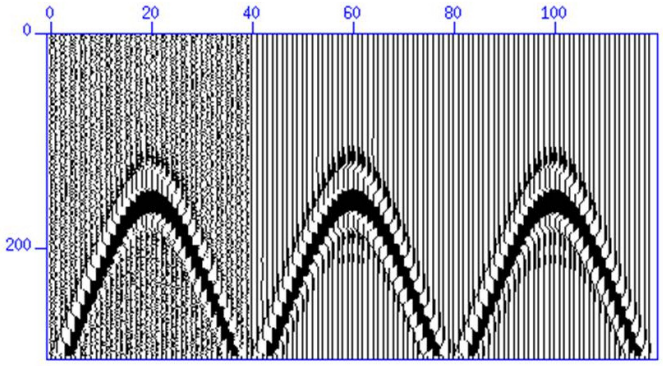

Figure 4. Traces 0-39 show the noisy model data used in the test for S/N=5; traces 40-79 show the model response of the initial guess of Q=15; traces 80-119 show the converged result of inversion after 3 iterations with Q=6.33. The inversion is nearly identical to a noise-free version of the data but the error of fit is slightly worse due to the noise.

We note from Figure 4 that noise has not greatly affected the FWI inversion result for this case of a modest S/N ratio. The converged value of Q is 6.33, although the error is slightly worse than for the noise-free case.

If we then use noisier data, with S/N = 2.5, we test the robustness further. Figure 5 shows this result. With the same initial guess, the inversion produces a result that is very close to the desired result, although the error of fit is worse than the previous cases.

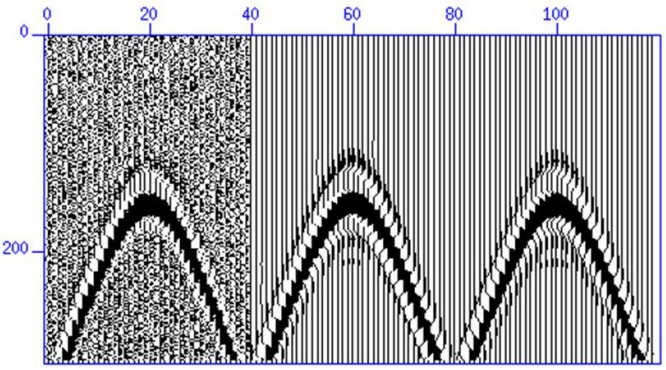

Figure 5. Traces 0-39 show the noisy model data used in the test for S/N=2.5; traces 40-79 show the model response of the initial guess of Q=15; traces 80-119 show the converged result of inversion after 3 iterations with Q=6.26. The inversion produces and excellent answer, but the error of fit is worse than the cases in Figures 3 and 4.

Table 1 gives a summary of the convergence of the inversions. We note that in all cases it took only 3 iterations to reach a very good estimate for Q, although the error of fit was greater in the noisier cases, as expected.

Iteration number	Value of Q (noiseless)	Error	Value of Q (noisy)	Error	Value of Q (very noisy)	Error
0(first guess)	15.00	.012005	15.00	.017965	15.0	0.15882
1	2.00	.061620	2.33	.052797	2.67	0.18959
2	4.48	.004056	5.15	.010938	4.80	0.14749
3	6.09	.000028	6.33	.006555	6.26	0.13638

Table 1: A comparison of the inversion results for the noiseless seismic section and the noisy seismic sections of Figure 2. It is interesting that for the first iteration in the noisy case, the value of Q is slightly better and the error is slightly less, than for the noiseless case.

A graph of the iterative inversion for the noiseless, noisy, and very noisy cases is shown in Figure 6. We notice that from this figure and the table that there is a steady improvement in the model from iterations 1 to 3, and that the inversion for Q values in all three cases is acceptably close to the true value of 6.28, despite the fact that the error of fit is worse as the noise increase (as expected). Despite the error of fit becoming worse with noise, the inversion for the noisy data may be slightly better than the noiseless case.

That is, the noise for these cases does not appear to have shifted the correct position of the local minimum. A graph of error for the various data sets and the various values of Q is shown in Figure 7. The position for the local minimum for various ranges of Q stays in about the same position and this is shown in Figure 7. To understand this better, we can plot the error of fit for the case of the noiseless data and the error of fit for the noisy data cases. We plot the errors for the three data sets for Q=2, 4, 6, 8 and 10 (Q values in the neighbourhood of the correct answer). The error values for Figure 7 are shown in Table 2. As expected, we note that the error of fit level is higher for the noisy seismic data than the noiseless data. The local minimum for the noisy case does not go below the noise level for our data. However, we also note that the local minimum of the error in all three cases is slightly greater than Q=6, near the true value of 6.28. Therefore it is not surprising that the iterative inversion for both data sets produces acceptable answers despite the fact that the error level is higher for the noisy case. The algorithm is a Gauss-Newton approach that seeks out the local minimum. The noise has not damaged the answer in this case.

Q value	Error for noiseless case	Error for noisy case	Error for very noisy case
2.0	0.06162	0.06938	0.09026
4.0	0.00768	0.01468	0.03480
6.0	0.00003	0.00661	0.02639
8.0	0.00144	0.00781	0.02729
10.0	0.00457	0.01077	0.03009

Table 2: The errors for the noiseless seismogram and the noisy seismogram are shown for various values of Q.

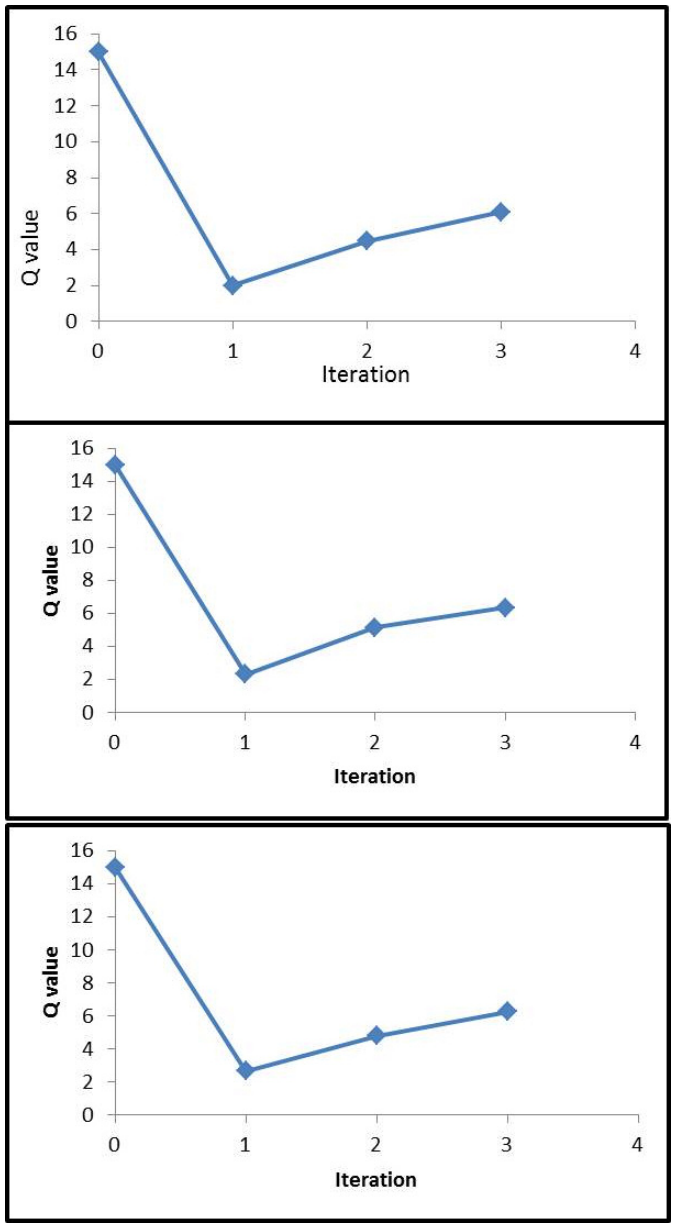

Figure 6. Iterative inversion for Q value of second layer for the case of the noiseless data (top figure) and the case of noisy data (middle figure) and the case of very noisy data (bottom). The top inversion gives a Q value of 6.09, the middle inversion gives a Q value of 6.33 and the bottom inversion gives a Q value of 6.26. The correct value is Q=6.28.

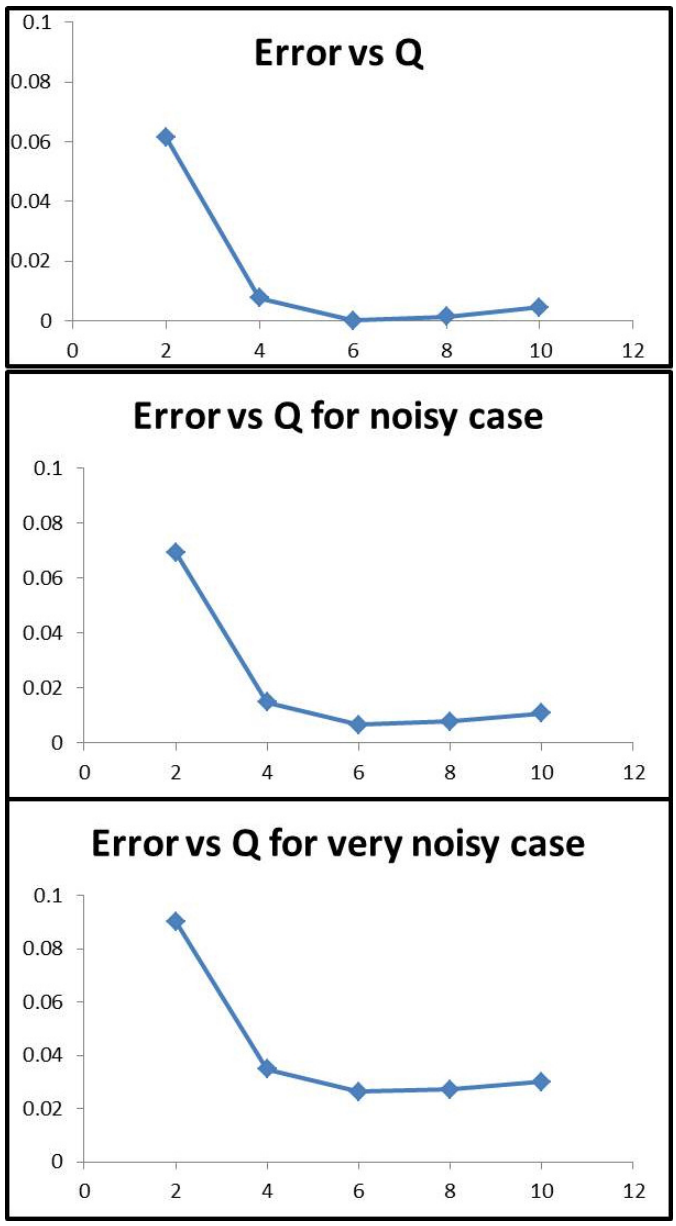

Figure 7. Error vs Q for the noise-free case (top). Error vs Q for the noisy case (middle) and for the very noisy case (bottom).

The reason for the robustness of our full waveform inversions in this simple example may lie in the fact that our additive noise was basically a set of random numbers with zero mean. Also the noise levels were modest (S/N=5 and S/N=2.5).

Further insight into the robustness can come from revisiting equation (8). Since the matrix **A** is rectangular, we can find a least squares solution to (8) by multiplying the equation by $\mathbf{A}^T$ to produce:

$$\mathbf{A}^T\mathbf{A}\mathbf{x}=\mathbf{A}^T\mathbf{b} \qquad (9)$$

Now if we consider the noisy data case we replace **b** by **b+n** and equation (9) becomes:

$$\mathbf{A}^T\mathbf{A}\mathbf{x}=\mathbf{A}^T\mathbf{b} + \mathbf{A}^T\,\mathbf{n}. \qquad (10)$$

However, if the noise is random and zero mean, the second term on the right hand side, $\mathbf{A}^T\,\mathbf{n}$, will tend to zero especially if **A** smoothly varying. This second term is essentially a crosscorrelation of a random sequence with one that is smoothly varying and its value will generally be small compared to the first term. This and the behavior of the error function have meant that the full waveform inversion is robust, at least for modest noise levels.

Conclusions

The estimation of oil viscosity is crucial for characterization of heavy oil fields. One of the methods of estimating viscosity is through inversion for seismic-Q. Q-tomography has been used for these inversions, but it may be worthwhile to follow tomography with full waveform inversion. One of the concerns with full waveform inversion is its sensitivity to noise in the data. In this short note, we examine the inversion of Q for noise-contaminated signals. From our initial computational experiments, it appears that full-waveform inversion has not been seriously affected by moderate amounts of additive noise. The robustness of full waveform inversion may come from the fact that the position of local minima for the correct Q values has not been changed. Also the lack of correlation of random noise with the data has not seriously damaged the solutions. More tests of robustness need to be done. However, for these initial tests, full waveform inversion appears to be robust for estimation of seismic-Q.

Acknowledgements

The authors wish to thank CHORUS (Consortium for Heavy Oil Research by University Scientists) for their financial support of this project. We thank Sven Treitel for his constructive suggestions and careful editing of this paper. Finally we thank Naimeh Riazi for assistance with the graphics and we thank Bee Bednar, Changoo Shin, and Enders Robinson for their constructive and encouraging reviews.

References

Aki, K., and Richards, P. 2002, Quantitative seismology, University Science Books.

Carcione, J. M., 2007, Wave fields in real media: Elsevier.

Dvorkin, J., and Nur, A., 1993, Dynamic poroelasticity: a unified model with the squirt flow and the Biot mechanism: Geophysics, 58, 524-533.

Dvorkin, J, Nolen-Hoeksema, R., and Nur, A., 1994, The squirt-flow mechanism: macroscopic description, Geophysics, 59, 428-438.

Lines, L., and Treitel, S., 1984, Tutorial: A review of least-squares inversion and its application to geophysical problems: Geophysical Prospecting, 32, 159-186.

Lines, L., Vasheghani, F., and Treitel, S., 2008, Reflections on Q, CSEG Recorder, December issue, 36-38.

Lines, L., Wong, J., Innanen, K., Vasheghani, F., Sondergeld, C., Treitel, S., and Ulrych, T., 2014, Research Note: Experimental measurements of Q-contrast reflections, Geophysical Prospecting, 62, 190-195.

McMechan, G., 1983, Seismic tomography in boreholes, Geophys. J.R. astr. Soc., 74, 601-612.

Pica, A., Diet, J.P., and Tarantola, A., 1990, Nonlinear inversion of seismic reflection data in a laterally invariant medium, Geophysics, 55, 284-292.

Quan, Y., and Harris, J. M., 1997, Seismic attenuation tomography using frequency shift method: Geophysics, 62, 895-905.

Shin, C.S. 1987, Nonlinear elastic inversion by blocky parameterization, Ph.D. thesis, University of Tulsa.

Shin, C.S., Pyun, S., and Bednar, J.B., 2007, Comparison of waveform inversion, part 1: conventional wavefield vs logarithmic wavefield, Geophysical Prospecting, v. 55, 449-464.

Spencer, T. W., Sonnad, J. R., and Butler, T. M., 1982, Seismic Q – stratigraphy or dissipation: Geophysics, 47, 16-24.

Toksoz, M.N., and Johnston, D., 1981, Seismic wave attenuation, SEG publication.

Vasheghani, F., and Lines, L., 2009, Viscosity and Q in heavy-oil reservoir characterization, The Leading Edge, 856-860.

Vasheghani, F., 2011, Estimating heavy oil viscosity from seismic data, Ph.D. thesis, University of Calgary.

Vasheghani, F., and Lines, L.R., 2012, Estimating heavy oil viscosity from crosswell seismic data, Journal of Seismic Exploration, 21, 247-266.

Zhou, C., Cai, W., Luo, Y., Schuster, G., and Hassanzadeh, S., 1993, High-resolution crosswell imaging by seismic travel time + waveform inversion, The Leading Edge, 988-991.